National Transportation Safety Board
Office of Research and Engineering
Washington, DC 20594

CEN22LA250

MATERIALS LABORATORY

Factual Report 22-102

March 17, 2023

(This page intentionally left blank)

A. INCIDENT INFORMATION

Location: Evansville, Indiana
Date: June 8, 2022
Vehicle: Beech 58, N78KL
Investigator: Mike Hodges (AS-CEN) and Clint Crookshanks (AS-40)

B. COMPONENTS EXAMINED

Propeller blade piece.

C. EXAMINATION PARTICIPANTS

Specialist — Matthew R. Fox, Ph.D.
NTSB
Washington, DC

Specialist — Nancy McAtee
NTSB
Washington, DC

D. DETAILS OF THE EXAMINATION

Overall views of the propeller blade piece as received are shown in figure 1. The blade was fractured 16.89 inches from the root end face. Stamped markings on the root end face indicated the propeller blade was a Hartzell part number FC7063Q propeller blade with serial number J51843. According to Hartzell build records, the propeller assembly manufacture date was October 9, 2000.

The blade had an electro-thermal de-icing boot installed on its leading edge. Manufacturing information stamped on the inboard end of the boot indicated that it was an Ice Shield part number SMR2271-10, manufactured under Federal Aviation Administration Parts Manufacturer Approval (FAA-PMA), with a cure date in the fourth quarter of 2009. As manufactured, the blade did not have a de-icing boot installed. However, the installation of the SMR Technologies (Ice Shield) de-icing boot is permitted under supplemental type certificate (STC) ST01468CH.

According to propeller maintenance records, the propeller had been installed new on November 12, 2002, by Colemill Enterprises in accordance with STC SA1762SO, which likely included installation of de-icing boots on the leading edges of the propeller blades. The propeller was overhauled on December 28, 2009, at 1,153.8 hours time since new, which would require removal of any de-icing boot that had been installed at that time. Given the cure date for the boot installed on the submitted blade piece, the boot on that blade at the time of fracture was likely installed at blade overhaul in 2009.

Airplane registration records indicate that the airplane was most recently sold on May 13, 2021. The last 100-hour inspection of the propeller occurred on January 10, 2022, when the propeller had 1,171.8 hours time since overhaul (TSO). The previous 100-hour inspection, completed before the airplane was sold, occurred on December 17, 2020, at 1,096.9 hours TSO. The propeller had accumulated 1,199.6 hours TSO at the time of the incident.

An overall view of the fracture surface is shown in figure 2. A portion of the fracture surface was oriented in a flat, chordwise plane consistent with fatigue. The fatigue region had faceted features with curving crack arrest lines, features consistent with fatigue crack growth. The fatigue features emanated from an origin area on the flat side of the blade near the middle of the chord as indicated in figure 2. The fatigue origin area was associated with a series of grooves in the blade surface adjacent to the trailing edge of the de-icing boot as shown circled in figure 3.

The leading edge of the blade within a couple inches of the fracture surface is shown in figure 4. In that area, the boot appeared fractured and disturbed in the circled area about 1.75 inches from the fracture surface. The boot was pulled away from the surface, revealing an impact mark in the blade as shown in the right image in figure 4. The geometry of the impact mark was different from the series of groove-like features observed with the fatigue origin anomaly shown in figure 3.

The blade piece was cut chordwise approximately 1 inch from the fracture surface to facilitate further examination of the fracture surface and the anomaly associated with the origin area. An oblique view of the anomaly and the adjacent fracture surface is shown in figure 5. The majority of the fatigue features emanated from an origin area at the leading edge of the anomaly, labeled the primary origin in figure 5. Unlabeled arrows on the fracture surface show local directions of fatigue crack propagation away from the primary origin area. Additional secondary origin areas were noted along the length of the anomaly in the area indicated with an unlabeled bracket in figure 5.

Before cleaning the fracture surface for a more detailed examination of fracture features, an examination of the surface coatings was completed using a scanning electron microscope (SEM). The surface coating at the anomaly was relatively thick and had multiple voids as shown in the upper image in figure 6. The fracture surface of the coating had a flat faceted appearance that appeared relatively uniform in texture across the thickness. In contrast, the coating on the flat side of the blade closer to the trailing edge had a thinner thickness with varying texture through the thickness as shown in figure 7.

The coating composition in the areas shown in figures 6 and 7 were also analyzed using energy dispersive x-ray spectroscopy (EDS), and the resulting spectra are shown in figure 8. The coating on the anomaly had high peaks of aluminum, oxygen, and carbon as shown in the upper spectrum in figure 8. In contrast, the

coating on the blade flat closer to the trailing edge had high peaks of silicon, magnesium, chlorine, carbon, and oxygen.

After the initial SEM and EDS examination of the coatings was completed, the fracture surface was rinsed using acetone. The coating on the anomaly appeared to soften with the exposure to acetone, so the surface cleaning process was interrupted to facilitate coating analysis using Fourier-transform infrared spectroscopy (FTIR). The samples were examined using an FTIR spectrometer with a diamond attenuated total reflectance (ATR) accessory in accordance to ASTM E1252-98 (American Society for Testing Materials E1252-98: *Standard Practice for General Techniques for Obtaining Infrared Spectra for Qualitative Analysis and American Society for Testing Materials*). The spectrometer was used to collect and process infrared wavelength absorbance spectra of the unknown material. Three areas on the sectioned piece of the blade were selected for further analysis; Area A (area of painted blade near the trailing edge); Area B (sealant at the trailing edge of de-icing boot) and Area C (an unknown material covering the anomaly). Three swab samples taken from Area C were also analyzed.

The spectrum for the sample from Area A contained the following combination of spectral peaks corresponding to particular functional groups found within molecular structure of the material. The presence of a very low broad peak at ~3500 cm^{-1} is indicative of an oxygen-hydrogen (O-H) functional group. The presence of a strong doublet peak between ~2920 $cm^{-1}$and ~2850 cm^{-1} is indicative of a carbon-hydrogen (C-H) single stretching bond. The presence of a single peak at ~1720 cm^{-1} is indicative of a carbon-oxygen (C=O) stretching double bond. The presence of a peak at ~1580 cm^{-1} is indicative of double bonded carbon (C=C) stretching bond (aromatic). The presence of a single peak at ~1460 cm^{-1} is indicative of a carbon-$hydrogen_3$ ($C\text{-}H_3$) asymmetric stretching bond. The presence of a single peak at ~1380 cm^{-1} is indicative of a carbon-$hydrogen_3$ ($C\text{-}H_3$) symmetric stretching bond. The presence of a single peak at ~1260 cm^{-1} is indicative of a carbon-oxygen (C-O) aromatic stretching bond. The presence of a doublet peak between ~1100 cm^{-1} and ~1030 cm^{-1} is indicative of a carbon-oxygen-carbon (C-O-C) stretching bond. The presence of a single peak ~820 cm^{-1} is indicative of a carbon-$hydrogen_3$ ($C\text{-}H_3$) bending bond. This combination of functional groups is consistent with an epoxide. A spectral library search was performed using the spectrum. The search found a match to several epoxy resins indicating that the propeller paint is likely an epoxy paint.

The spectrum from Area B contained the following combination of spectral peaks corresponding to particular functional groups found within molecular structure of the material. The presence of a low broad peak at ~3440 cm^{-1} is indicative of an nitrogen-hydrogen (N-H) functional group. The presence of a strong triplet peak between ~2960 cm^{-1}, ~2920 cm^{-1}, and ~2870 cm^{-1} is indicative of a carbon-hydrogen (C-H) stretching bonds. The presence of a strong single peak at ~1730 cm^{-1} is indicative of

double bonded carbon-oxygen (C=O) stretching bond. The presence of a strong single peak at ~1650 cm^{-1} is also indicative of double bonded carbon-oxygen (C=O) stretching bond (secondary polyurethane). The presence of a single peak ~1450 cm^{-1} is indicative of a carbon-hydrogen$_2$ ($C-H_2$) asymmetric stretching bond. The presence of a single peak at ~1380 cm^{-1} is indicative of a carbon-hydrogen$_3$ ($C-H_3$) symmetric stretching bond. The presence of a single peak at ~1270 cm^{-1} is indicative of a carbon-carbon-oxygen-carbon (C-C(O)-C) (ether) stretching bond. The presence of a single peak ~1140 cm^{-1} is indicative of a carbon-oxygen (C-O) aromatic stretching bond. The presence of a doublet peak between ~1060 cm^{-1} and ~990 cm^{-1} is indicative of a carbon-oxygen-carbon (C-O-C) stretching bond. The presence of a single peak at ~840cm^{-1} is indicative of a carbon-hydrogen$_3$ ($C-H_3$) bending bond. The presence of a single peak at ~660 cm^{-1} is indicative of a nitrogen-hydrogen (N-H) bond. This combination of functional groups is consistent with a urethane. A spectral library search was performed on the spectrum. The search found similarities to several polyurethane adhesives and resins, which is consistent with a filler specified by the de-icing boot manufacturer.

The spectra from Area C contained the following combination of spectral peaks corresponding to particular functional groups found within molecular structure of the material. The presence of a low broad peak at ~3200 cm^{-1} is indicative of an oxygen-hydrogen (O-H) functional group. The presence of a strong triplet peak between ~2950 cm^{-1}, 2930 cm^{-1}, and ~2870 cm^{-1} is indicative of a carbon-hydrogen (C-H) single stretching bond. The presence of a single peak at ~1720 cm^{-1} is indicative of a carbon-oxygen (C=O) stretching double bond. The presence of a peak at ~1650 cm^{-1} is indicative of double bonded carbon (C=C) stretching bond (aromatic). The presence of a single peak at ~1450 cm^{-1} is indicative of a carbon-hydrogen$_3$ ($C-H_3$) asymmetric stretching bond. The presence of a single peak at ~1360 cm^{-1} is indicative of a carbon-hydrogen$_3$ ($C-H_3$) symmetric stretching bond. The presence of a doublet peak between ~1270 cm^{-1} and ~1240 cm^{-1} is indicative of a carbon-oxygen (C-O) aromatic stretching bond. The presence of a peak at ~1020 cm^{-1} is indicative of a carbon-hydroxy (C-OH) stretching bond. The presence of a single peak at ~840 cm^{-1} is indicative of a carbon-hydrogen$_3$ ($C-H_3$) bending bond. The presence of a single peak at ~740cm^{-1} is indicative of a ring substitution stretching bond. The presence of a single peak at ~660cm^{-1} is indicative of an oxygen-carbon-hydroxy (O-C-OH) bond. This combination of functional groups is consistent with an aromatic epoxide. A spectral library search was perform using the spectrum. The search found similarities to several epoxy resins consistent with epoxy paints. While a similar material, the unknown material from Area C is not the same paint found in Area A.

Next, the sectioned piece with the fracture surface was submerged in acetone and cleaned using an ultrasonic cleaner, and a view of the fatigue region on the cleaned fracture surface is shown in figure 10. A portion of the fracture surface had a darker appearance with a smooth curving boundary, consistent with fatigue crack growth. Relatively smoother features consistent with stable crack growth continued

slightly beyond the dark region, and unlabeled arrows indicate the extent of the stable crack growth region. As the crack grew through the thickness, it grew faster toward the leading edge than toward the trailing edge, leaving the origin area skewed closer to the trailing edge of the stable fatigue crack growth region. In the region beyond the arrows, the fracture surface had a rougher texture and duller appearance but remained in a flat plane consistent with a transition to unstable progressive crack growth. The progressive growth extended to the leading edge and to the camber surface, ending at the dashed line in figure 10. The remainder of the fracture showed rough, matte gray features consistent with ductile overstress fracture.

The anomaly at the fatigue origin is shown in the lower image in figure 10 after the coating had been removed with acetone. The anomaly consisted of multiple parallel grooves with rounded bottoms. The original surface coating (paint) was missing from the surfaces of the grooves, but remnant areas of black coating that appeared to be paint was observed on the peaks between the grooves such as the areas indicated in the lower image in figure 10. A black sealant with a rubbery texture was observed over the paint at the trailing edge of the de-icing boot, and both the sealant and the paint appeared to be disturbed from the groove surfaces of the anomaly. Neither the paint nor the rubbery sealant was easily removed with acetone.

The fracture surface was further examined using the SEM, and resulting images are shown in figures 11 through 15. A montage of images showing an overall view of the origin area and the anomaly is shown in the upper image in figure 11, and closer views of the origin areas are shown in the lower images in figure 11 and in figure 12. The primary origin, shown in the lower image in figure 11, was located at the flat face of the blade near the leading edge of the anomaly. The fracture surface at the origin was damaged adjacent to the flat surface, but unlabeled arrows indicate local propagation directions consistent with the primary fatigue origin at the location indicated. Secondary origin areas were located along the edge of the anomaly closer to the trailing edge in the area shown in figure 12. Unlabeled arrows in figure 12 indicate local crack directions with crack features emanating from the secondary origin area indicated with a bracket. However, these cracks soon merged with the primary crack front. Typical fatigue fracture features consistent with high-cycle fatigue were observed within the stable fatigue region such as the areas shown in figures 13 and 14. Striations such as those shown in figure 15 were observed in the region of unstable progressive growth (between the arrows and camber surface or dashed line shown in figure 11).

A montage of SEM images of the flat surface adjacent to the fracture surface showing the anomaly at the fatigue origin is shown in figure 16. Portions of the anomaly surface such as those indicated with the yellow arrows appear white in the

image due to charging.[1] The area indicated by the uppermost yellow arrow in figure 16 was analyzed using EDS, and the resulting spectrum is shown in figure 17. The spectrum showed high peaks of silicon, magnesium chlorine, carbon, and oxygen, consistent with paint (see paint spectrum in figure 8). The paint was observed on the peaks between the grooves for the anomaly. In areas with less paint covering the surface, the paint filled spanwise scratches in the surface. During blade manufacture, the surface is sanded spanwise, and similar spanwise scratches were observed in other undisturbed areas of the blade surface.

Sliding contact marks were observed at the bottoms of the grooves, and red arrows in figure 16 indicate the local direction of the sliding contact. A lip of disturbed material was observed at the outboard trailing edge of the marks such as the lip indicated in figure 16. Closer views of features associated with the anomaly are shown in figures 18 and 19. Spanwise scratch marks at the peaks between the grooves continued along the sides of the groove consistent with an impression into the surface, and the surface at the deepest portion of the groove had a smeared surface consistent with sliding contact. The inboard flank of the outboard groove had curved sliding contact marks as shown in figure 18, and spanwise marks on the peaks between the grooves were deformed toward the trailing edge at the outboard edge of the peak consistent with sliding contact along the inboard flank of the groove.

The grooves had a curved profile both in the nearly spanwise direction and facing the flat face. Measurements of the radii of curvature of anomaly features in two orientations are shown in figure 20. In the upper image, the feature was oriented such that the plane of the measured radii was approximately perpendicular to the viewing direction. Radii of the peaks for two of the grooves measured 0.349 inch and 0.529 inch. The deepest part of the groove for the two grooves intersecting the fracture surface intersected the same circle as shown with a radius of 0.357 inch. Curvature of the inboard flank on three of the grooves was measured on the flat face as shown in the lower image in figure 20. The radii measured 0.531 inch, 0.574 inch, and 0.483 inch.

[1] Charging is the accumulation of negative charge on the surface that develops during electron imaging of nonconductive material in an SEM under high vacuum and can result in overexposure and/or distortion in the image.

A 3-dimensional image of the anomaly was obtained using a Keyence VHX 7000 in depth mode. The sample was tilted to optimize viewing on the flank surfaces on either side of the grooves. Next, a depth profile along a linear trace through the middle of the anomaly was obtained. Results of the analysis are shown in figure 21. The profile at the lower side of figure 9 shows several grooves with varying depths relative to the outside surface. The overall shape of the grooves where the flanks transitioned to the peak appeared to be more rounded on the outboard flank and had a more abrupt transition on the inboard flank.

Submitted by:

Matthew R. Fox, Ph.D.
Chief Technical Advisor - Materials

Figure 1. Overall views of the submitted propeller blade piece.

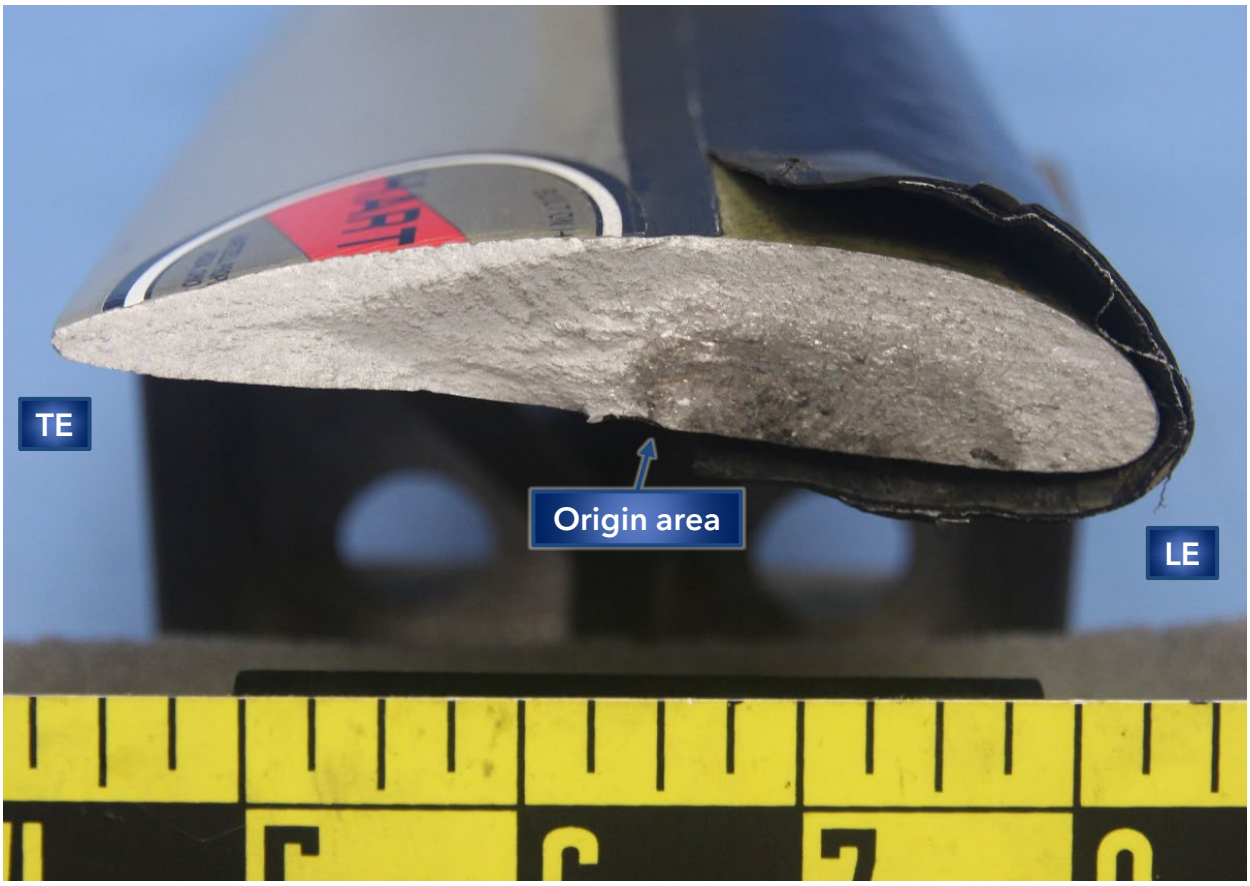

Figure 2. Fracture surface of the propeller blade piece as received.

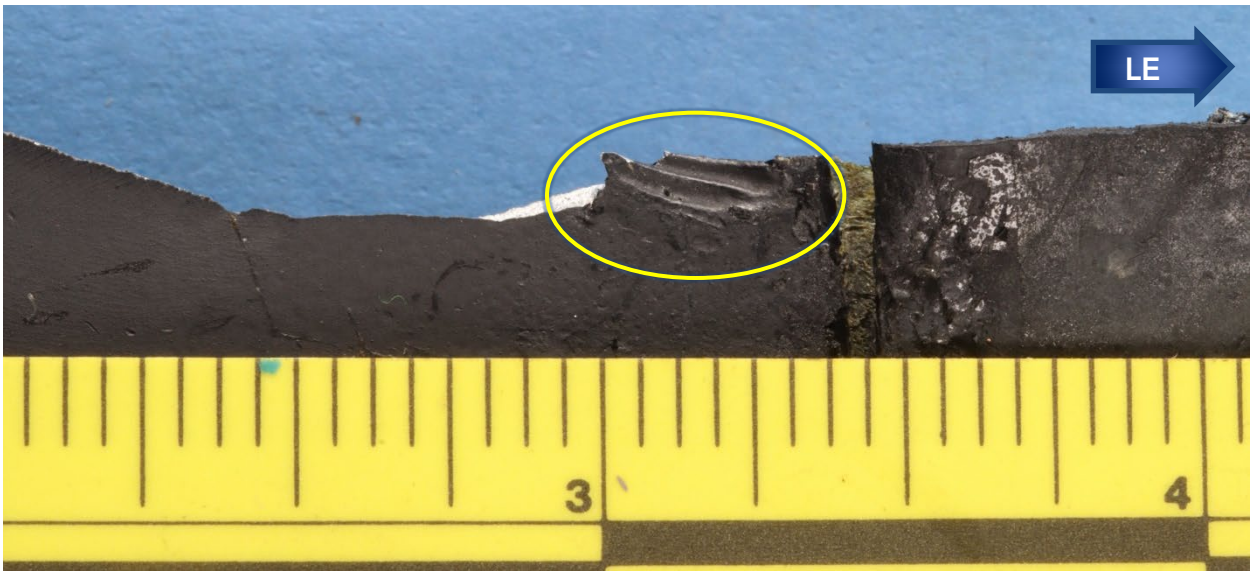

Figure 3. Closer view of the anomaly (circled area) on the flat side of the blade.

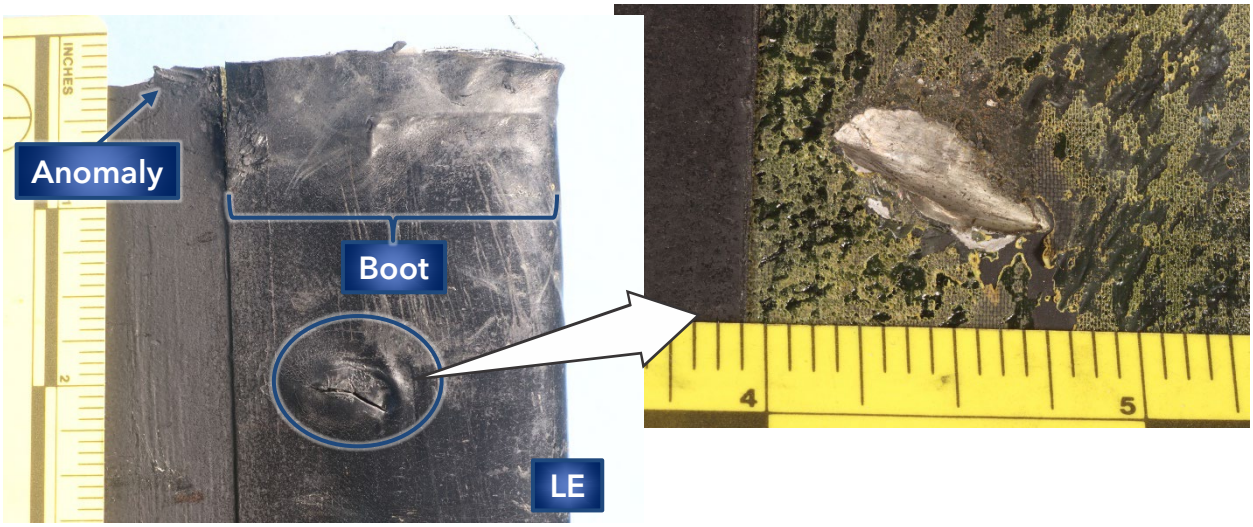

Figure 4. Flat side of the blade showing an anomaly at the fatigue origin area and a tear in the boot near the fracture surface (left) and a view of the damage where the boot tear was observed after removing the boot (right image).

Figure 5. Oblique view of the anomaly. Arrows indicate the direction of fatigue features emanating from the primary origin at the leading end of the anomaly. A bracket indicates an area of secondary fatigue origins.

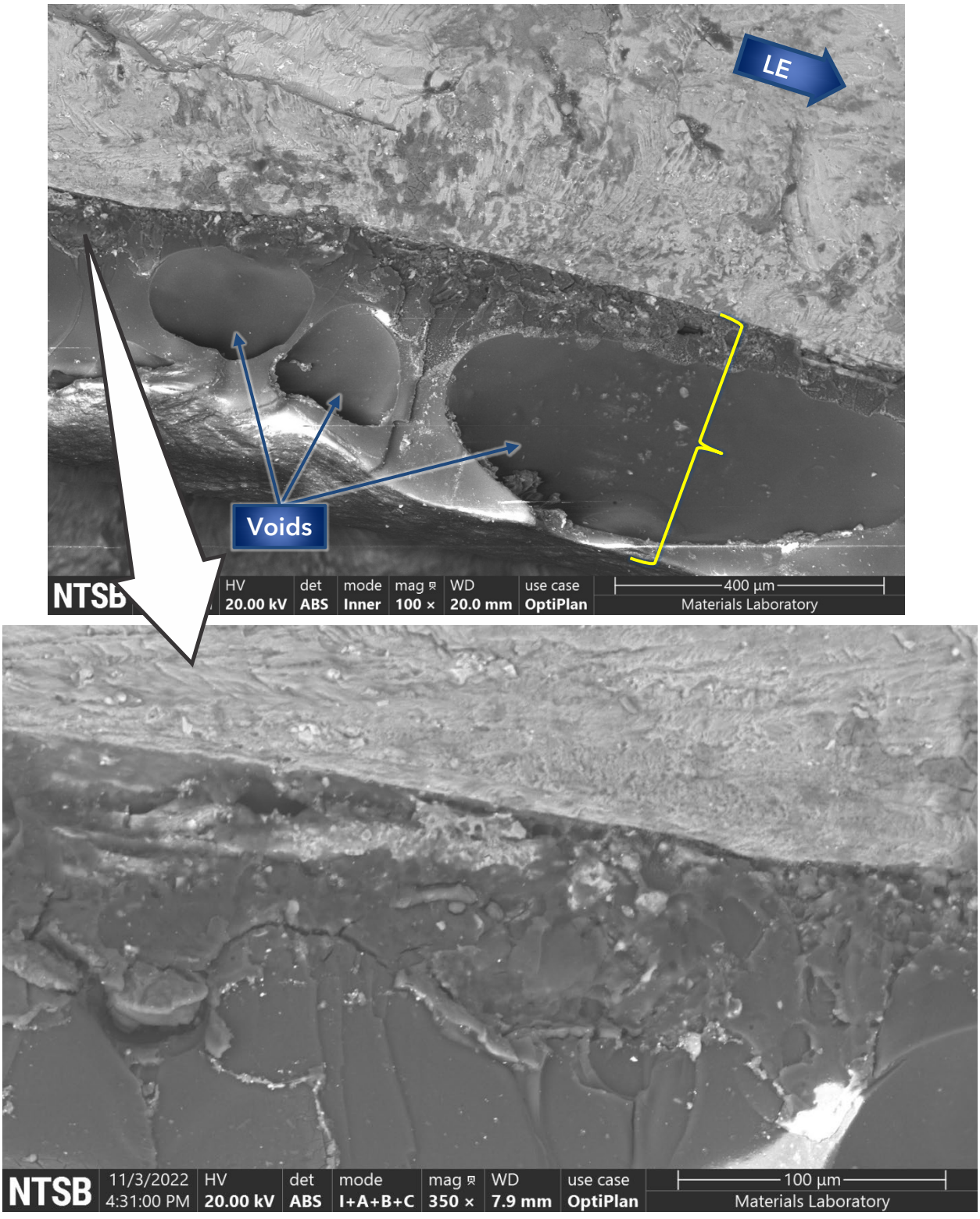

Figure 6. SEM images of the coating on the anomaly as viewed using a backscatter detector in composition mode. A bracket in the upper image indicates the thickness of the coating, and the arrow emanates from the area shown at higher magnification in the lower image.

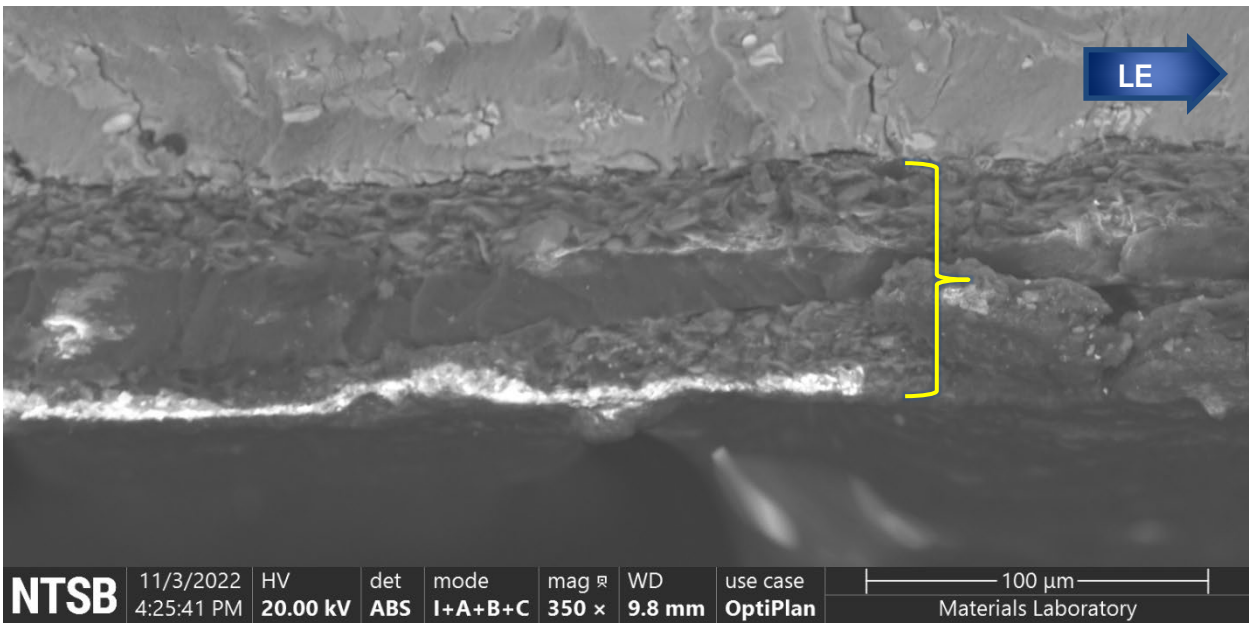

Figure 7. SEM image of the coating on the flat side of the blade away from the anomaly as viewed using a backscatter detector in composition mode. A bracket in the upper image indicates the thickness of the coating.

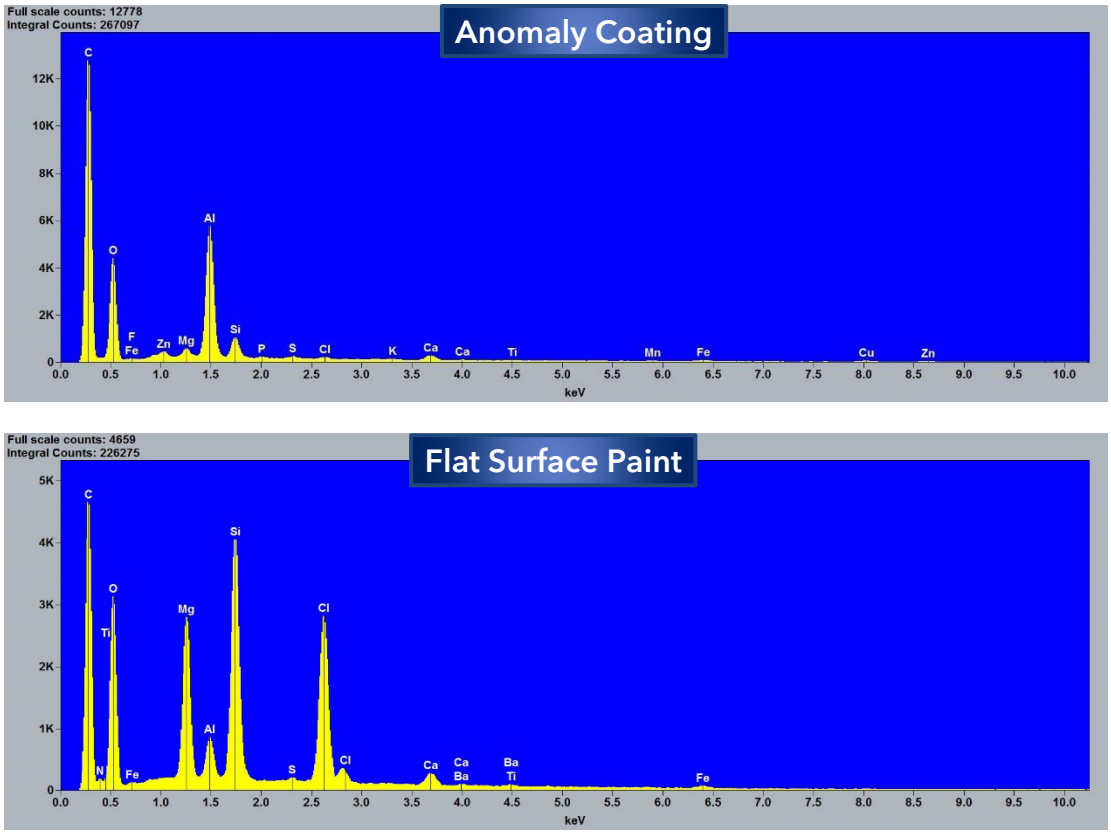

Figure 8. EDS spectra of the coating on the anomaly shown in figure 6 (upper spectrum) and on the flat side of the blade shown in figure 7 (lower spectrum).

Figure 9. Stitched optical image of the origin area after an acetone rinse.

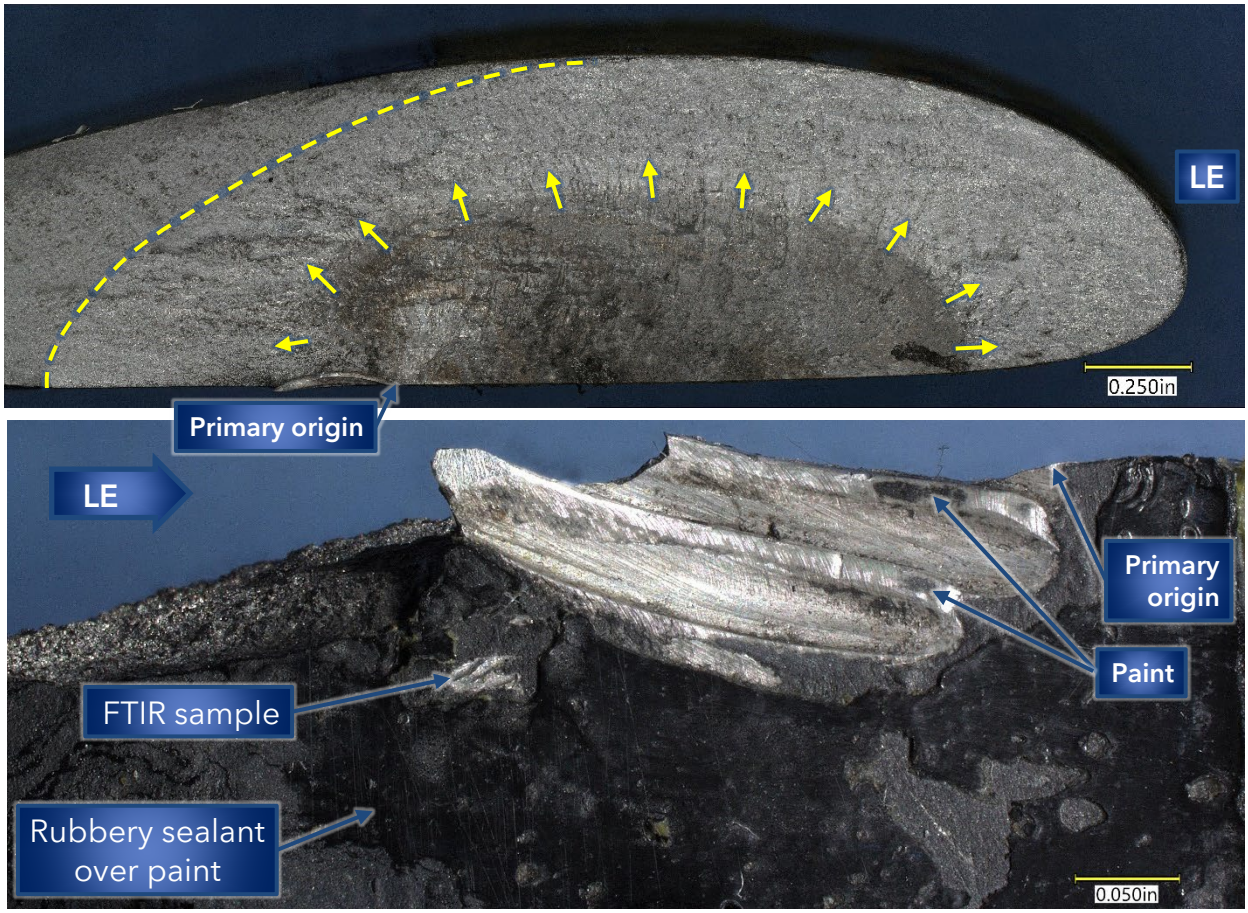

Figure 10. Fracture surface (upper image) and anomaly (lower image) after swabbing and ultrasonic cleaning with acetone. Arrows in the upper image indicate steady crack growth fracture features, and a dashed line indicates the extent of progressive crack growth.

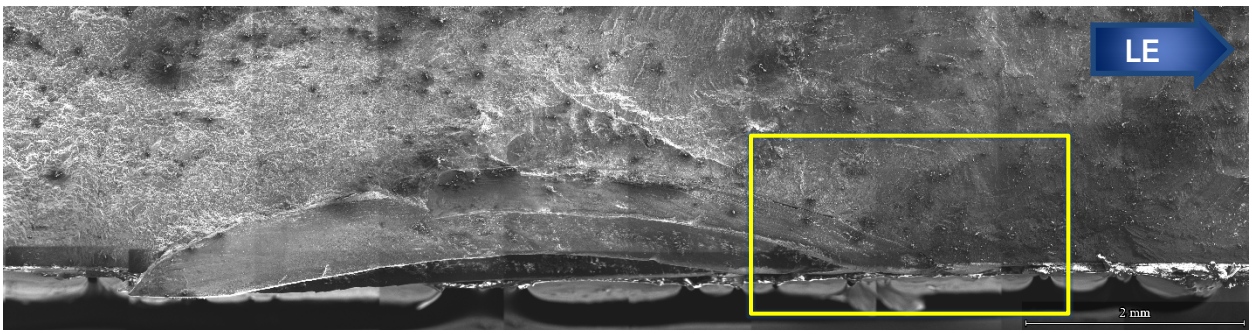

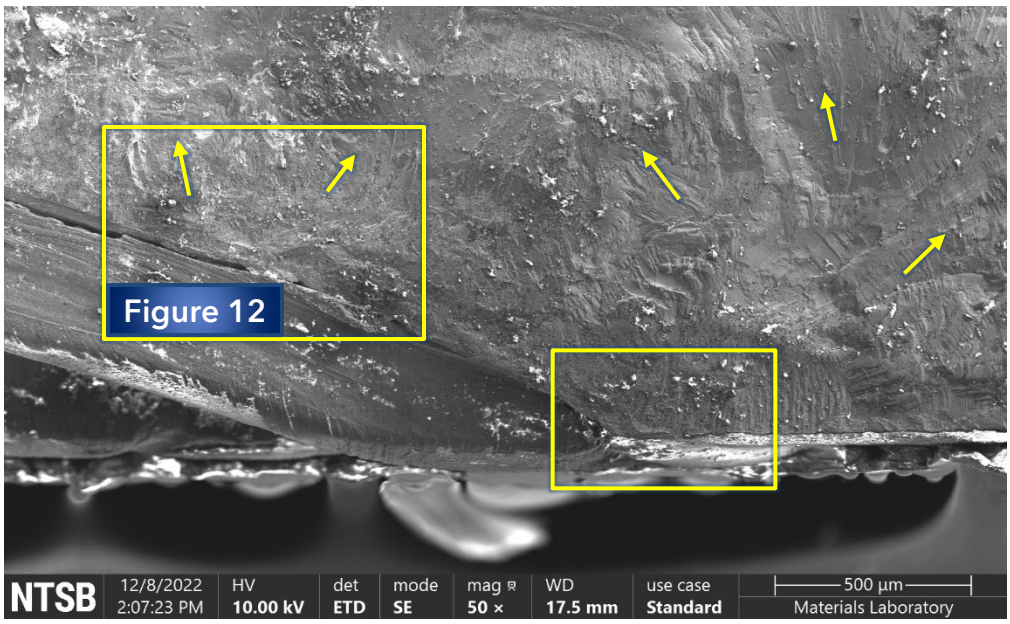

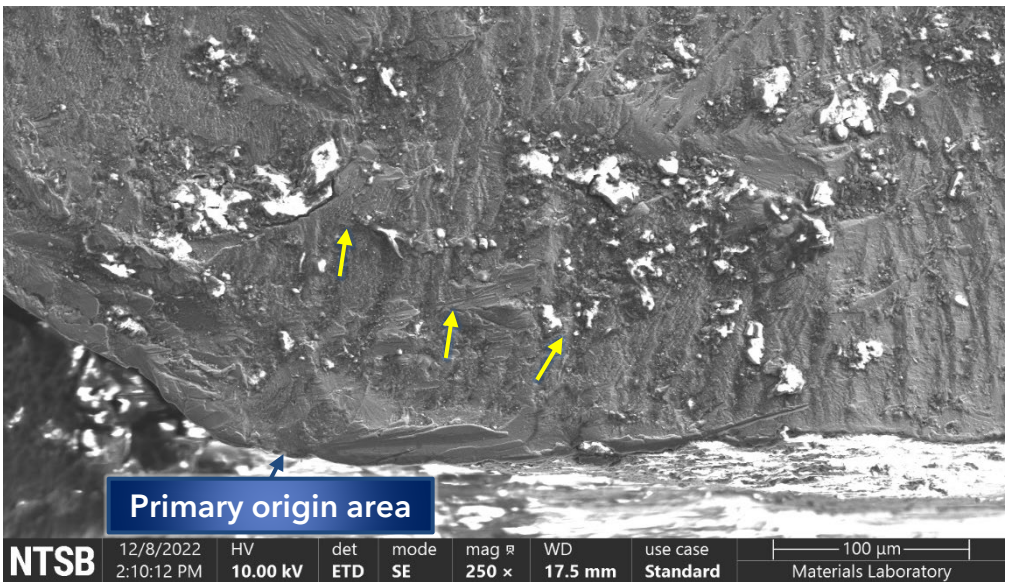

Figure 11. SEM images of the primary origin area after ultrasonic cleaning with acetone. The upper image is a stitched montage, and rectangles indicate areas shown magnified in subsequent images in this figure and in figure 12. Unlabeled arrows indicate local directions of fatigue crack growth.

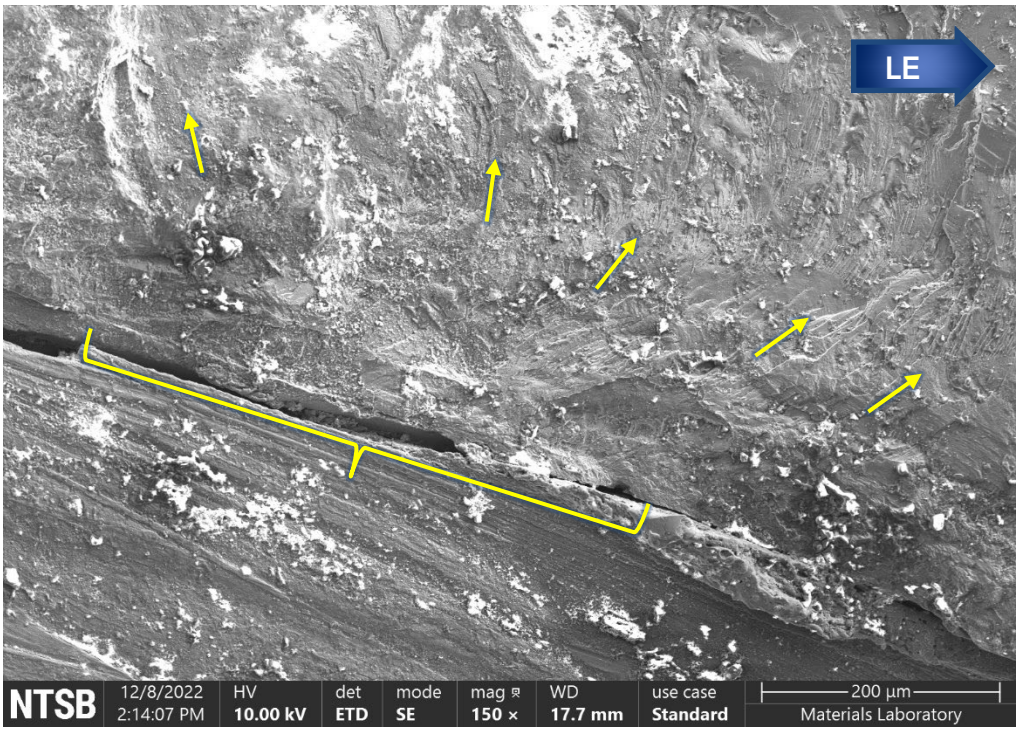

Figure 12. Secondary origin area (indicated with a bracket) emanating from the anomaly in an area trailing the primary origin area. Unlabeled arrows indicate the local direction of fatigue crack growth.

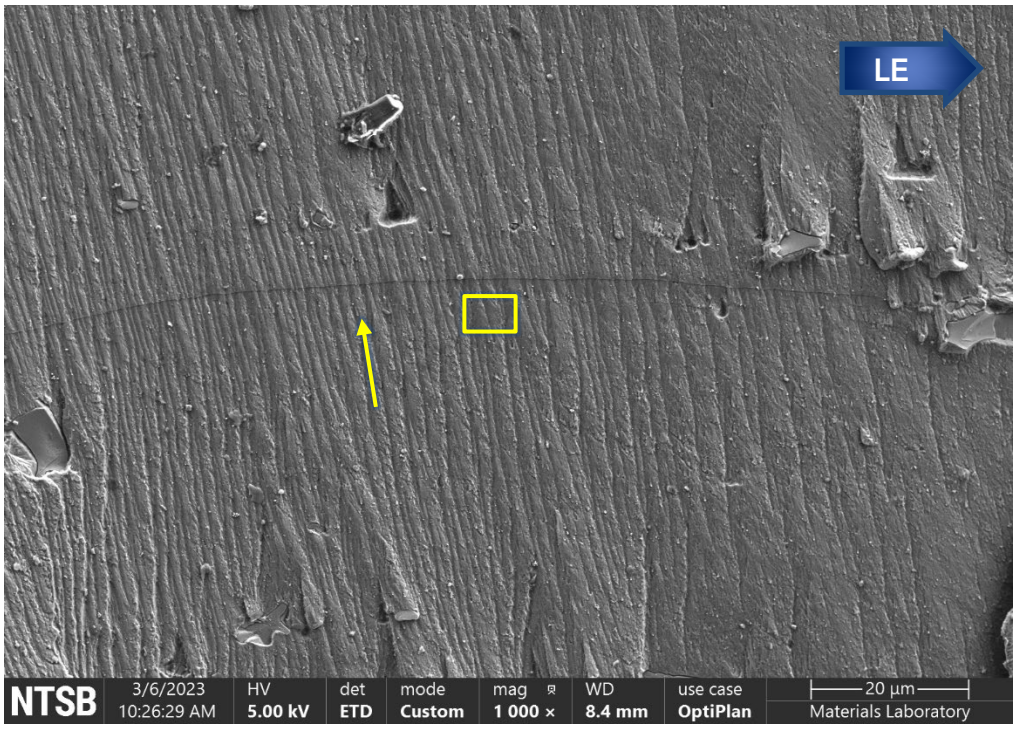

Figure 13. Typical fatigue features within the region of stable fatigue crack growth approximately 0.157 inch from the primary origin. An unlabeled arrow indicates the direction of crack growth, and the rectangle indicates the area shown at higher magnification in the next figure.

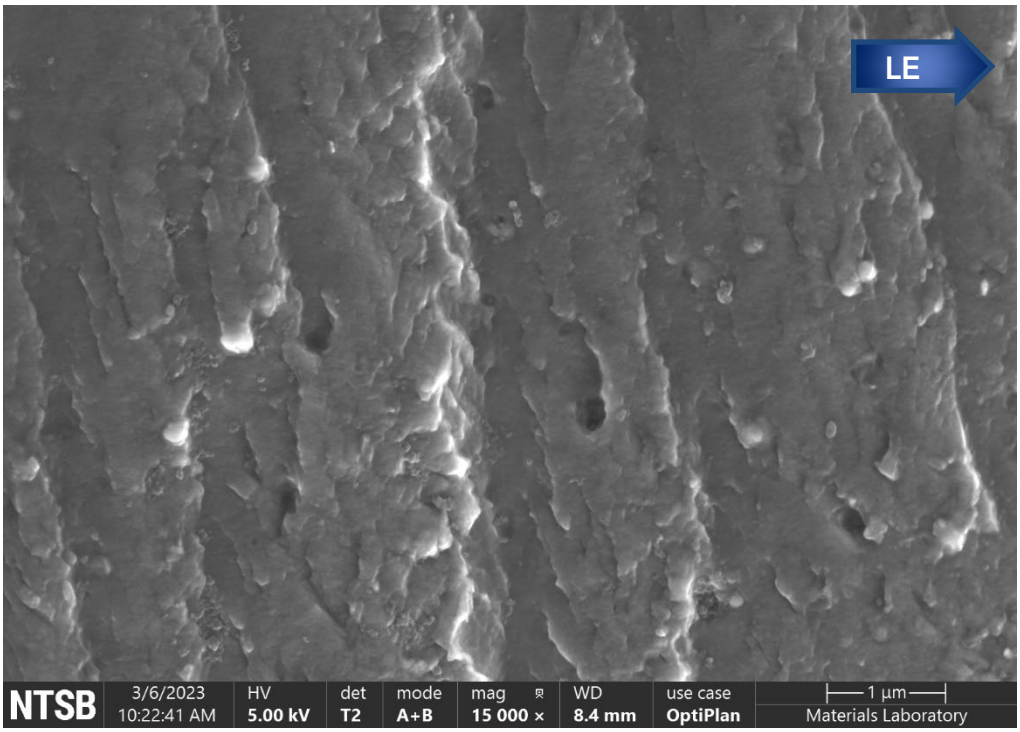

Figure 14. Fatigue features within the region of stable fatigue crack growth in the rectangle shown in the previous figure.

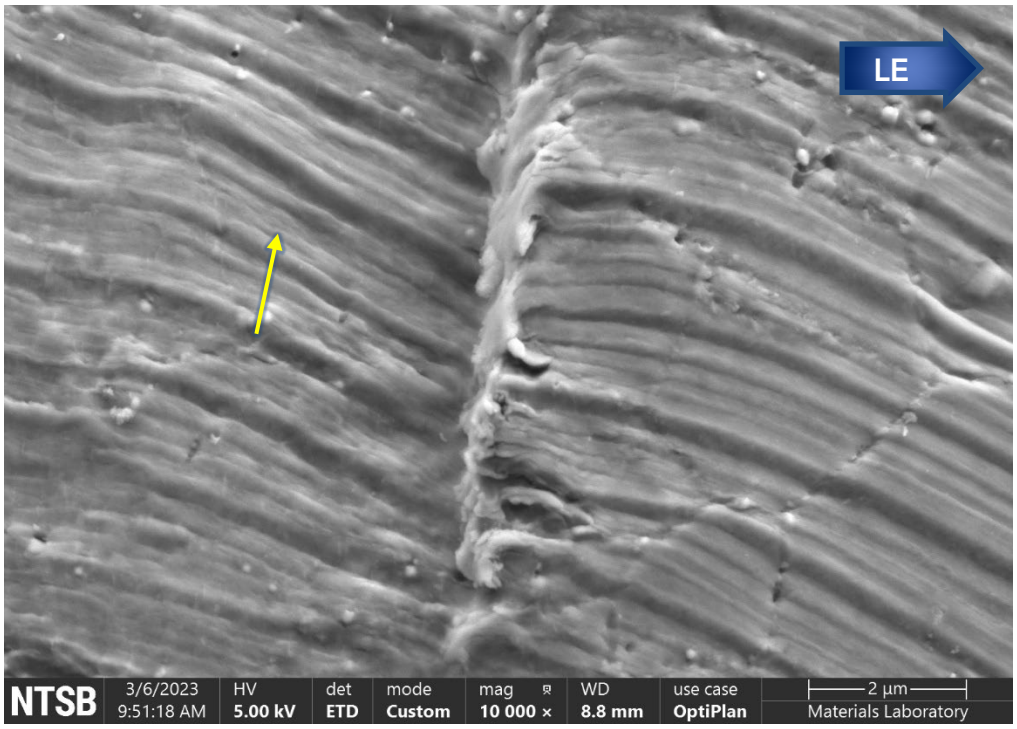

Figure 15. Typical fatigue features in the region of unstable fatigue crack growth. An unlabeled arrow indicates the direction of crack growth.

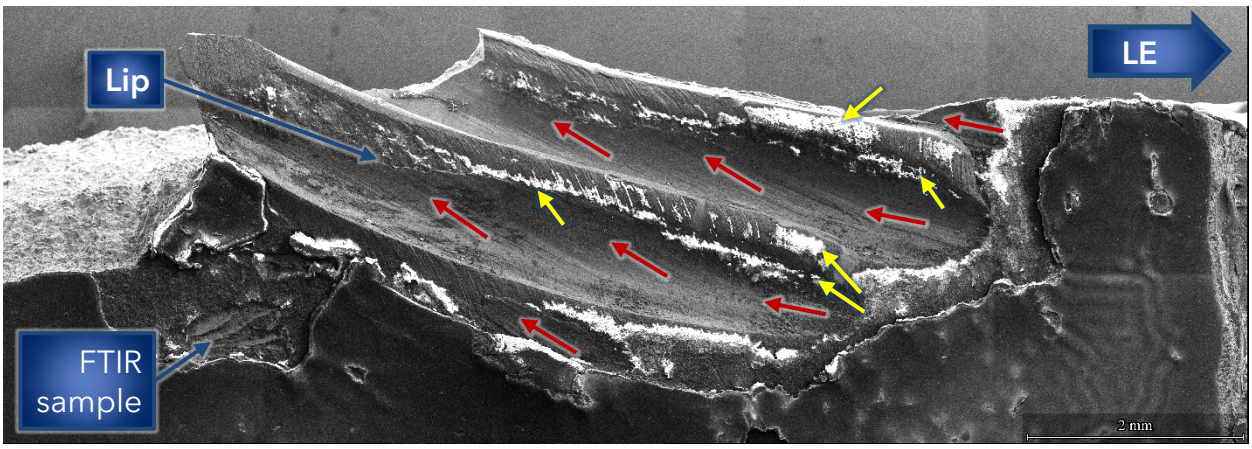

Figure 16. Anomaly after ultrasonic cleaning with acetone. Yellow arrows indicate some paint deposits, and red arrows indicate the direction of sliding contact.

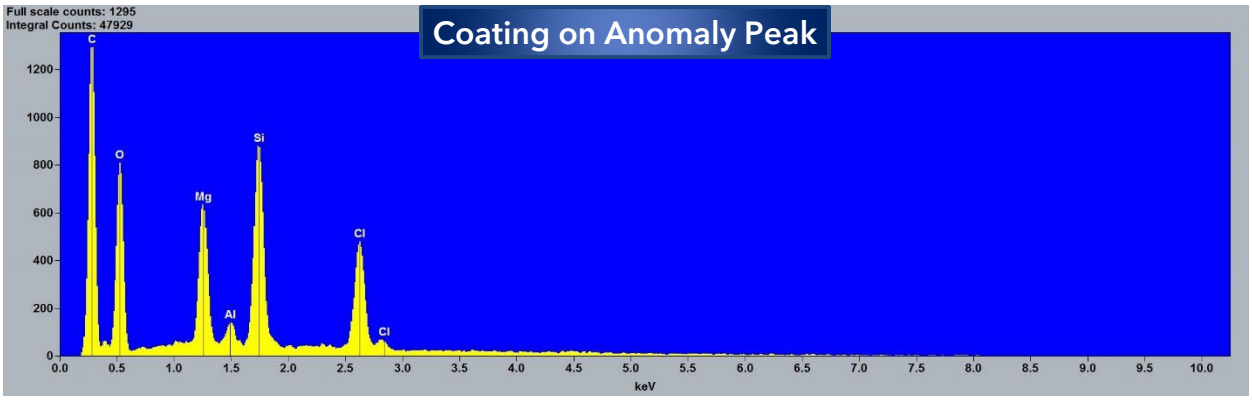

Figure 17. EDS spectrum for a coating on the anomaly peak (uppermost yellow arrow in figure 14) after ultrasonic cleaning with acetone.

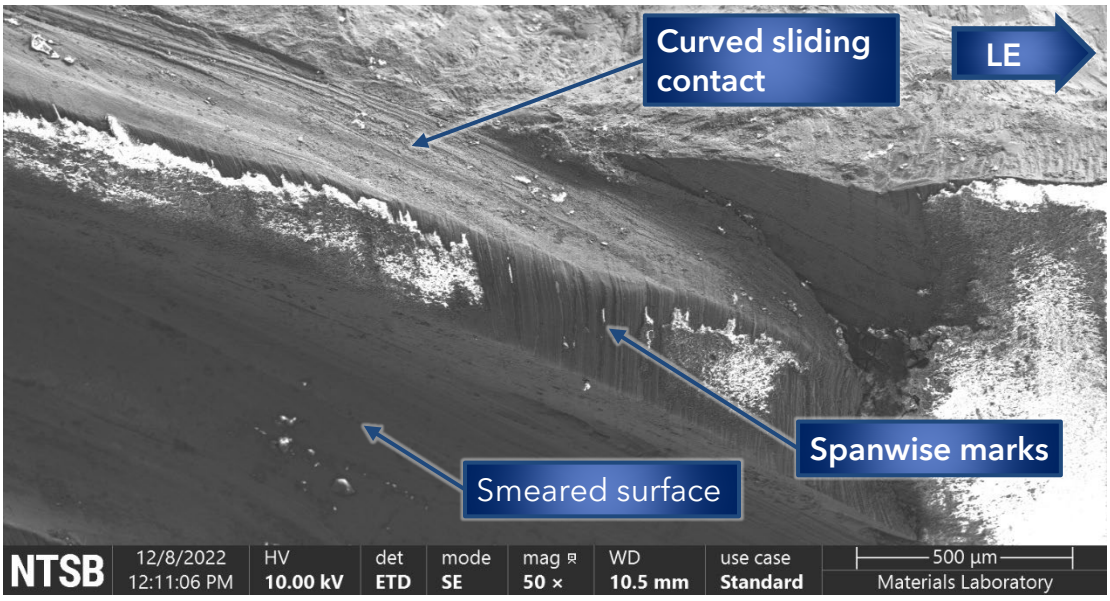

Figure 18. SEM image of the leading edge of the anomaly after ultrasonic cleaning with acetone.

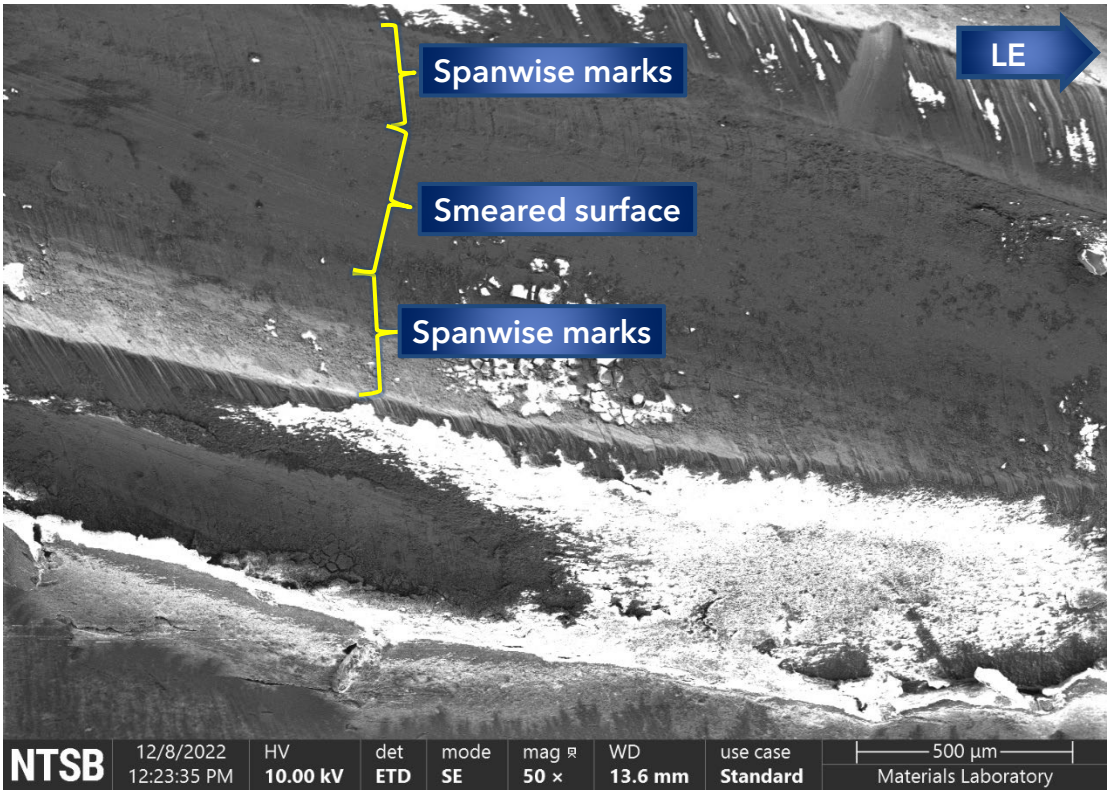

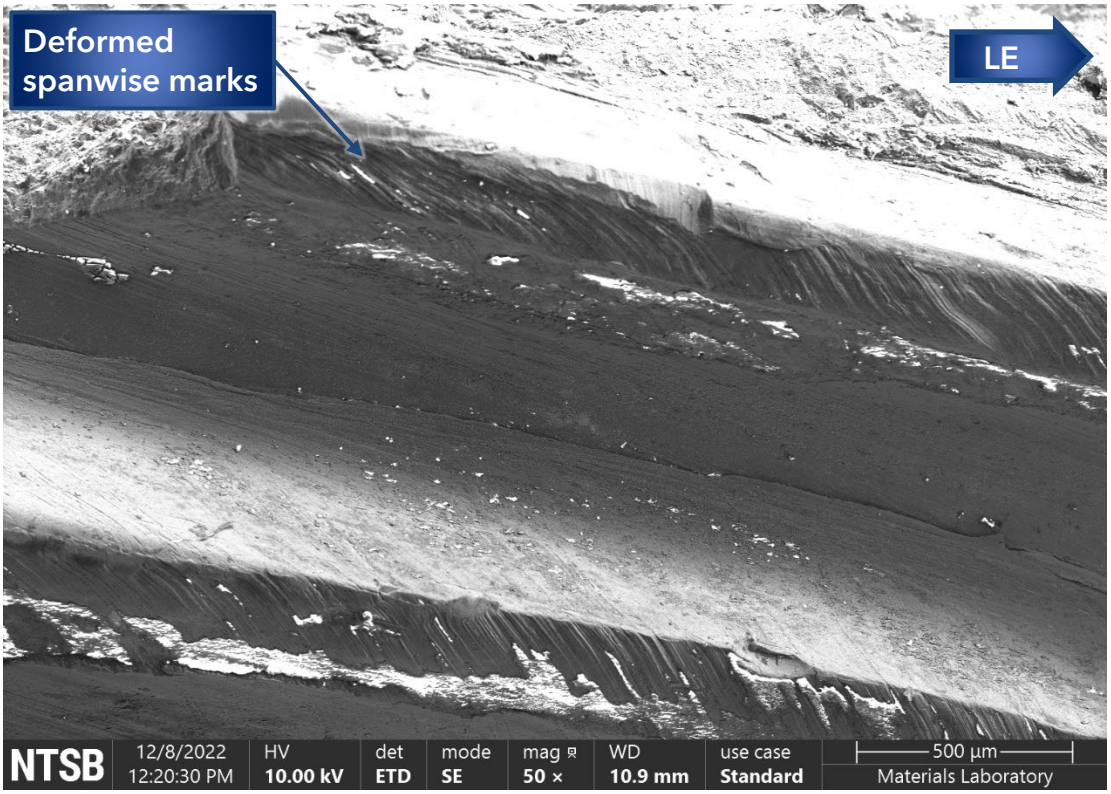

Figure 19. SEM images of the anomaly after ultrasonic cleaning with acetone.

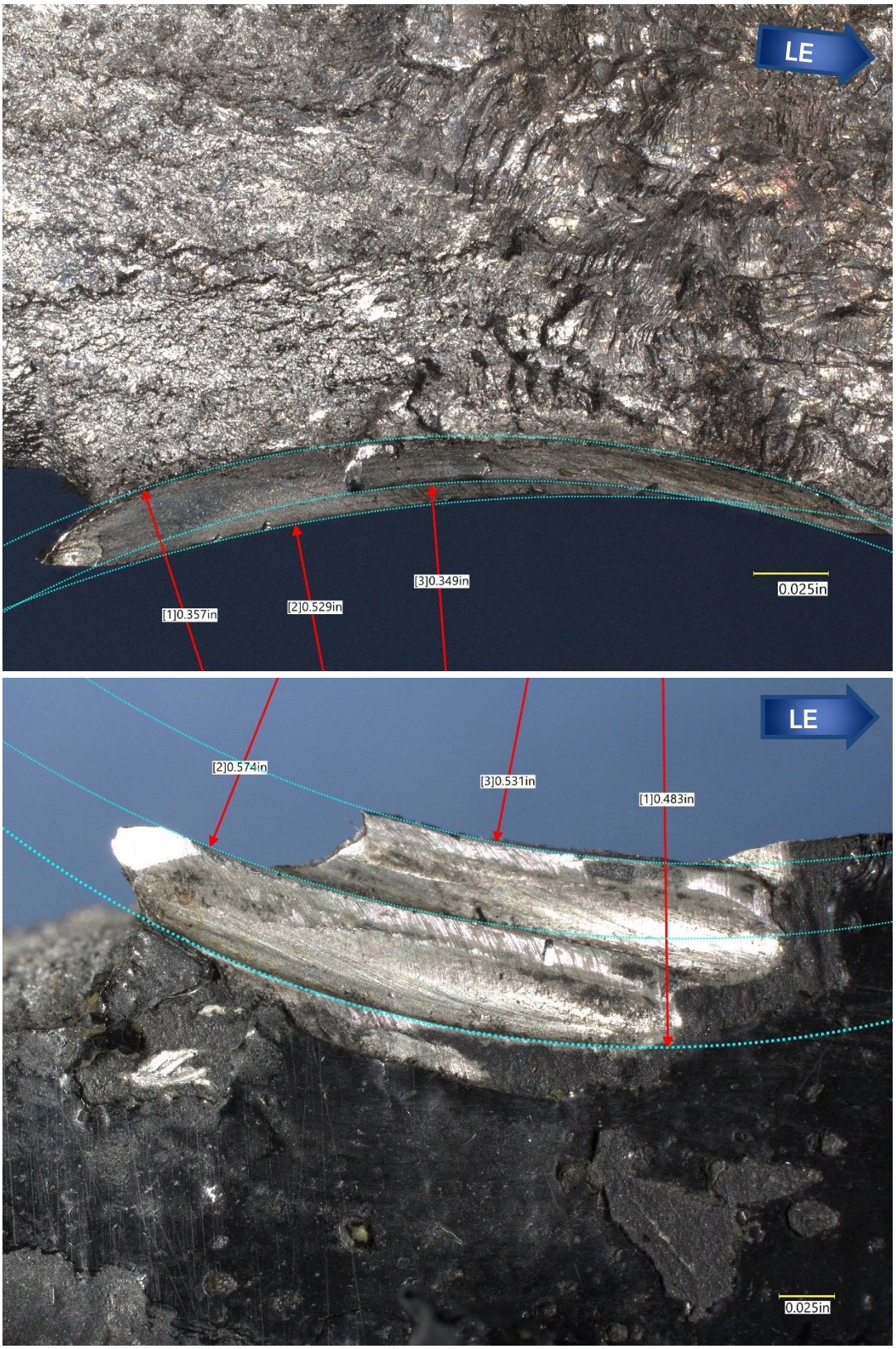

Figure 20. Radii of curvature measured on a nearly spanwise plane viewed approximately perpendicular to the anomaly flanks (upper image) and in a plane approximately parallel to the blade flat (lower image).

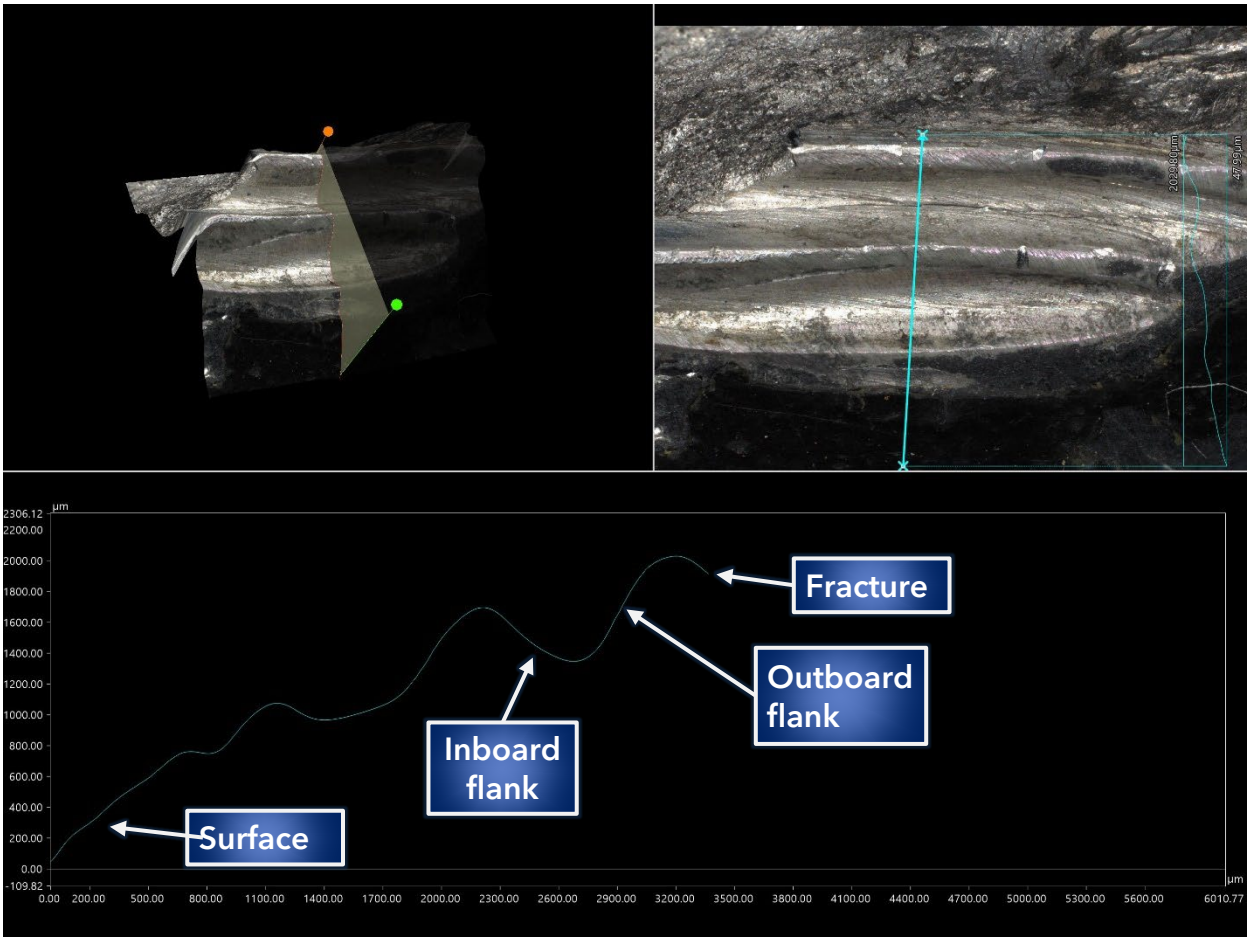

Figure 21. Three-dimensional profile of the anomaly obtained using a Keyence VHX 7000 in depth mode. In the chart, the vertical axis ranges from 0 to 2306 microns at 200-micron intervals, and the horizontal axis ranges from 0 to 6011 microns starting with a 200-micron interval followed by 300-micron intervals.